

Molecular Dynamics Simulation of the Effects of Anionic–Nonionic Surfactants on Interfacial Properties of the Oil–Water Interface

Zhaojun Chen,* Yangwen Zhu, Jinpan Zhong,* Ping Liu, Yougi Wang, Hongmin Yu, Li Zhang, Luxuan Ma, Deshuai Sun, and Kai Xia



Cite This: *ACS Omega* 2025, 10, 11325–11333



Read Online

ACCESS |



Metrics & More

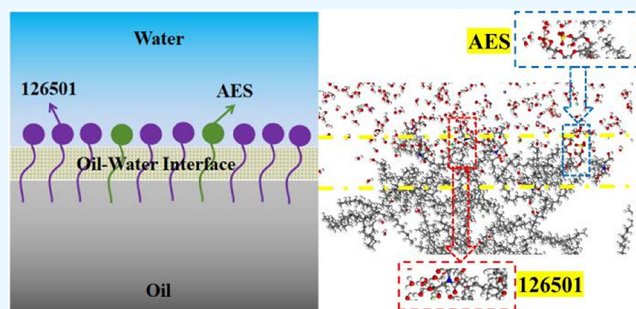


Article Recommendations



Supporting Information

ABSTRACT: Surfactant oil drive is a crucially enhanced oil recovery method that improves oil recovery rates. The aggregation behavior of surfactant molecules at the oil–water interface significantly influences oil repulsion. In this study, a molecular dynamics simulation is used to investigate this repellent behavior of single and binary surfactants of alkanolamides (6501) and fatty alcohol polyoxyethylene ether sodium sulfate (AES). The oil–water interface is characterized by density distribution, interfacial thickness, radial distribution function, interfacial tension, and interfacial generation energy. The results reveal that the dodecanolamide surfactant (126501) and AES effectively reduce interfacial tension. In the binary 126501/AES system, the interfacial film thickness increases to 18.08 Å, and the diffusion coefficient increases to 0.186 Å²/ps. The radial distribution function shows that oil molecules are located 4.2 Å from the anionic head of AES, which weakens the intermolecular forces within the oil layer. In the 126501/AES system, the interfacial energy of −96.12 kJ/mol indicates a stable interface. Moreover, both the 126501/AES and tetradecanolamide surfactant (146501)/AES systems exhibit excellent resistance to metal ions. The molecular-level mechanism provides useful guidance for designing the surfactant systems for enhanced oil recovery.



1. INTRODUCTION

Petroleum is an important nonrenewable resource. With growing global energy demand, crude oil consumption is projected to increase by 12.9% by 2035, reaching 109 million barrels per day.¹ However, the annual crude oil production does not keep pace with this increasing demand.² In fact, after primary and secondary recovery, 67% of the crude oil remains unrecovered in the reservoir,^{3,4} highlighting the importance of tertiary recovery. In tertiary recovery, the injection of chemicals into the reservoir to enhance the interactions among oil, water, and rock can improve the mobility of the oil, increasing the oil recovery rate to 80%.^{5,6} Chemical flooding, a key method of tertiary recovery, relies on surfactants, which have amphiphilic properties.^{7,8} These surfactants accumulate at the oil/water interface, forming a directed arrangement of surface layers that reduces the interfacial tension.^{9,10} This reduction in tension enhances the mobility of residual oil in the reservoir, making surfactants essential for improving oil recovery efficiency.¹¹ The structures of the surfactants affected the oil recovery efficiency. Pal et al.¹² investigated the oil recovery behavior of the anionic surfactants from coconut oil and found that they were stable in the presence of alkali and salt. Nonionic surfactants were widely used due to their excellent salt resistance but were limited by their poor temperature resistance. However, anionic–nonionic surfactant

systems exhibited good salt resistance and excellent stability,^{13,14} which could form the mixed adsorption layer at the oil and water interface by the synergistic effect and benefit the low interface tension.¹⁵

Currently, experimental methods for studying microscopic mechanisms are limited by detection time and spatial scales, making it challenging to directly observe molecular aggregation and related processes. As a result, computer simulations have emerged as an effective approach for investigating such issues, providing dynamic and structural information at the molecular level.^{16,17} Molecular dynamics (MD) simulations, in particular, have been widely used to provide detailed visualizations of molecular interactions, study the behavior of surfactants at the oil–water interface, and investigate the phenomena of aggregation and their effects on interfacial tension. These studies contribute to the development of the microscopic theories of oil recovery and provide a theoretical basis for the application of surfactant molecules.^{18,19} Compared to tradi-

Received: December 10, 2024

Revised: February 20, 2025

Accepted: March 7, 2025

Published: March 13, 2025



tional experimental methods, MD simulations can capture rapid dynamic processes under various temperature and pressure conditions and predict the long-term behavior of systems.²⁰

Researchers have extensively studied the impact of hydrophilic groups on the interfacial and adsorption properties of surfactants.²¹ Wu et al.²² investigated the effect of hydrophilic groups of surfactants on the interfacial properties of oil/water. By comparing the experimental data with the results of the MD simulation, they demonstrated that the MD simulation could effectively describe the ability of surfactants to reduce the interfacial tension at the oil/water interface at the microscopic level. Xu et al.²³ found that the capability of four surfactants reducing interfacial tension followed the order of fatty alcohol polyoxyethylene ether sodium sulfate (AES) > SDBS > SDS > SDSn. Moreover, the addition of oxygen, benzene ring, and oxyethyl in head groups enhanced the interaction between headgroup and water molecules. Shi et al.⁷ examined the microscopic behaviors of the anionic, nonionic, zwitterion, and gemini surfactants at the oil/water interface through MD simulations. The results showed that these surfactants formed stable adsorption membranes at the interface, with the gemini surfactant exhibiting the most powerful ability to reduce the interfacial tension than others. Jang et al.²⁴ explored the effect of molecular architecture of a surfactant, particularly the attachment position of benzenesulfonate on the hexadecane backbone at the decane–water interface. When benzenesulfonate in surfactant was in position of the fourth carbon (4-C16), it could form the most stable interface with the lowest interface formation energy, which was attributed to the fact that the effective length of the 4-C16 alkyl tail (9.53 ± 1.36 Å) was closest to that of decane (9.97 ± 1.03 Å).

The combined use of surfactants offers enhanced reduction of oil–water interfacial tension due to their superior stability and physicochemical properties.²⁵ Xian et al.²⁶ reported that increasing the content of sodium lauryl polyether carboxylate (anionic surfactant) between it and alkyl glycoside (APG-10) improved the interfacial activity and the interfacial stability of the composite system. Zhou et al.²⁷ found that the sulfate group in AES molecules attracted dodecyltrimethylammonium chloride molecules in the mixed surfactants, which reduced the repulsion between molecules and facilitated the formation of stable interfacial films at the interface. The zwitterionic/anionic surfactants also showed efficient improvement in interfacial stability. However, the appropriate hydrophilic–lipophilic balance and suitable structure of zwitterionic compounds are essential for anionic surfactants to achieve optimal lipophilic and hydrophilic groups when cooperating with betaine.²⁸

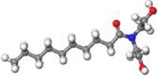
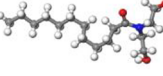
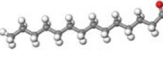
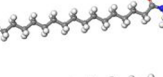
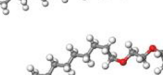
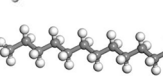

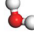
At present, the description of the interaction between the surfactant and oil molecules is still at the empirical level. It is difficult to determine the strength of the interaction between the hydrophilic groups of surfactants and oil molecules, which may be caused by dispersion effects.²⁹ This would greatly limit the understanding of structure–function correlations and hinder the design of surfactant molecules in the oil drive process. In this paper, we used an anionic nonionic surfactant AES with low manufacturing cost and high surface activity and nonionic surfactants with alkanolamides (6501) of different alkyl chain lengths. The MD simulation was used to study the effects of both pure and mixed surfactants on the interfacial behavior at the oil–water interface and elucidate the interfacial aggregation structures and the microscopic mechanisms of oil repulsion. A detailed analysis was conducted on how the

number of alkyl chains in the mixed surfactant system influences the interfacial performance. Additionally, the salt resistance of the mixed surfactants was examined.

2. SIMULATION AND EXPERIMENT

2.1. Simulation Setup. MD simulations were performed using Materials Studio (MS) (2020).³⁰ The structures of anionic and nonionic surfactants (AES and 6501 with different straight alkyl chains (10–18 carbons)) were constructed and optimized geometrically using the Forcite module³¹ under the Compass II force field.^{32,33} The geometry-optimized molecular models are shown in Table 1.

Table 1. Optimized Structure of Surfactant Molecules

Name	Molecular formula	Molecular structure
106501	C ₁₄ H ₂₉ NO ₃	
126501	C ₁₆ H ₃₃ NO ₃	
146504	C ₁₈ H ₃₇ NO ₃	
166501	C ₂₀ H ₄₁ NO ₃	
186501	C ₂₂ H ₄₅ NO ₃	
AES	C ₁₆ H ₃₃ O ₆ NaS	
C12	C ₁₂ H ₂₆	
H ₂ O	H ₂ O	

MD simulations were performed using the Amorphous Cell package, which is a part of MS (2020). The n-dodecane molecules were used as the crude oil model, and inorganic salts of CaCl₂, MgCl₂, and NaCl molecules were used as the brine model. The simulation system included oil, water, and surfactants. The oil box had a size of 30 × 30 × 30 nm³ and contained 100 oil molecules, while the water box was 30 × 30 × 40 nm³ and comprised 1000 water molecules. In the salt resistance process, inorganic salts of CaCl₂ (1 molecule), MgCl₂ (1 molecule), and NaCl (10 molecules) were added into water. All surfactant layers were located in the water layer. The MD model was constructed by stacking the surfactant aqueous solution/oil/surfactant aqueous solution from top to bottom using the Build Layer tool in MS.

2.2. Simulation Methods. MD simulations were carried out in the Forcite module in MS software. Due to high energy of the optimized box, the system was cooled down five times using Anneal^{10,26} (Anneal is a package within Materials Studio, specifically designed for optimizing material structures and understanding their thermal properties.) to obtain a low-energy oil/water/surfactant system at room temperature.

Then, isothermal–isobaric NPT ensemble calculations with 500 ps were conducted to relax the system. The Coulomb and van der Waals forces were calculated using Ewald's method with an intercept radius of 12.5 Å.^{34,35} The simulation temperature was maintained at 335 K and controlled by an Andersen thermostat and a Berendsen voltage regulator. The decay constant was selected as 0.1 ps, and the initial velocity of the molecules was randomly generated for 50,000 ps. The detailed parameters are given in Table S1. Subsequently, MD simulation systems were optimized with an NVT isothermal ensemble to determine the energy, radial distribution, density distribution, interfacial tension, and other parameters. The interfacial and phase behaviors of the surfactants in the presence of ions were then analyzed. Figure 1 shows the equilibrium configurations of the oil–water reference system. The number of molecules in the system is shown in Table S2.

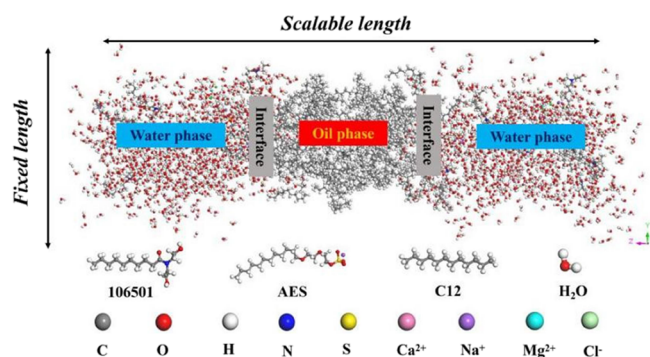


Figure 1. Surfactant/oil/water systems.

2.3. Experimental Section. The experiment consists of two main components: determination of the interfacial tension at the oil–water interface and the water separation rate of emulsions. The interfacial tension experiments were conducted at a temperature of 60 °C with a total mineralization of 20,000 mg/L. The interfacial tension values between various surfactant solutions and crude oil were measured using a TX500C spinning drop tensiometer.

3. RESULTS AND DISCUSSION

3.1. Interfacial Characteristics of Single Surfactants.

To better understand the distribution of surfactants at the oil–water interface, Figure 2 shows the density profiles of the surfactants along the Z-axis. The 50 and 90 Å regions corresponded to the interface of the oil–water layer. Figure 2a illustrates that the interfacial layer was very thin in the system without surfactants. Upon introducing surfactants, transition regions formed, where water and oil molecules exhibited a certain degree of mutual solubility due to the presence of surfactants, leading to the formation of interfacial films between water and oil layers. The relative density distributions of interfacial films at the oil–water interface varied significantly among five 6501 systems with different carbon chain lengths. In Figure 2b, surfactant 106501 predominantly resided in the aqueous phase, with minimal distribution at the interface. Conversely, Figure 2c shows that the relative density distribution at the interface was maximized in the 126501 system, indicating that 126501 was primarily concentrated in the interfacial film. Figure 2b–f reveals that surfactants with either too few or too many carbon atoms adversely affected the retention of surfactants at the interfacial film, consequently

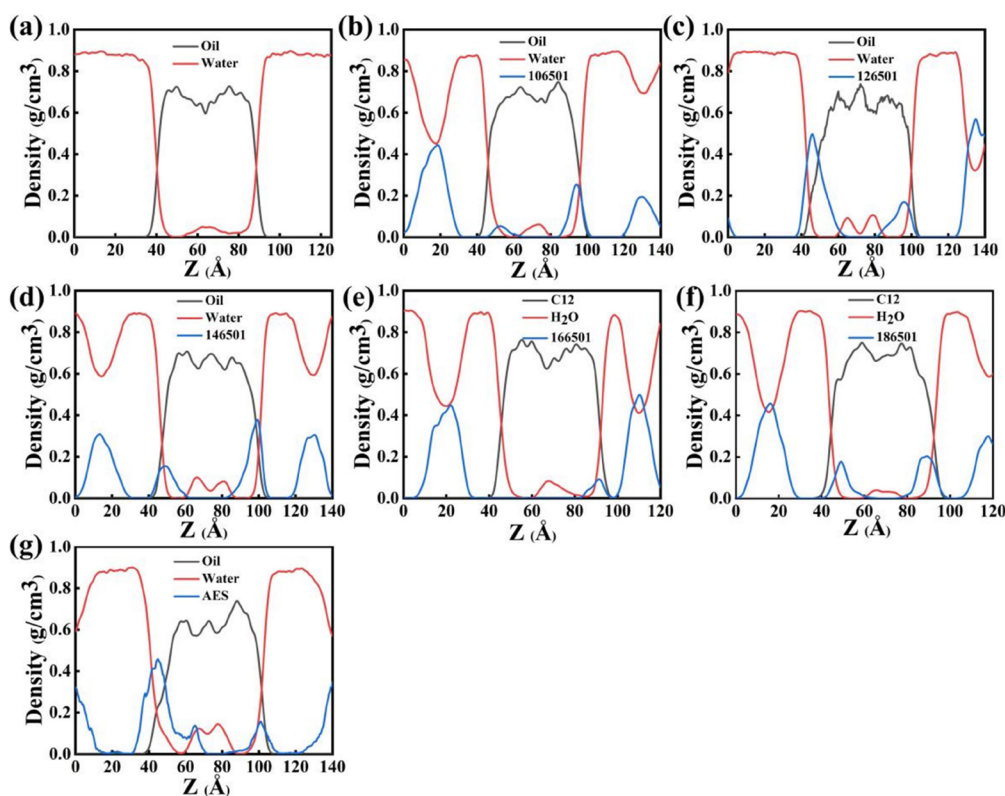


Figure 2. Density distribution of a single surfactant at the oil/water interface: (a) no surfactant, (b) 106501, (c) 126501, (d) 146501, (e) 166501, (f) 186501, and (g) AES.

impairing the development of a strong relative density distribution. Figure 3 shows the experimental results of

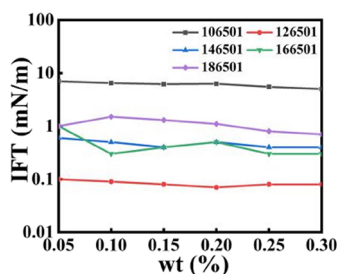


Figure 3. Effect of 6501 mass fractions on the interfacial tension of oil/water.

interfacial tension and also indicates that surfactant 126501 was more effective in reducing the oil–water interfacial tension. The reason may be that the carbon chain of the 126501 surfactant is close to that of crude oil. Therefore, the simulation results aligned with the experimental surface tension data are shown in Figure 3. Figure 2g presents the distribution of AES in the oil–water phases, showing an increase in the interfacial thickness and higher relative density at the interface. Consequently, both 126501 and AES are identified as the optimal surfactants for oil–water emulsification.

Figure 4 presents the density distribution in the Z-direction of the binary 6501/AES system, which was similar to that of the single surfactant systems. Compared to the single-component surfactant system, the density of surfactants in the binary systems showed a slight increase, indicating a larger interfacial thickness.^{36,37} The interfacial thickness (t_{total}) can be calculated according to the “90–90%” principle, as shown in Figure 5a.²⁵ t_{total} is defined as the distance between the points where the water/oil thickness curve reaches 90% of the system’s average thickness.³⁸ t_{water} and t_{oil} represent the thickness of the water layer and oil layer at the interface, respectively, which is calculated according to the “10–90%” principle. t_{oil} and t_{water} are defined as the distance between the

points at which the density curve of water or oil reaches 90 and 10% of the system’s water or oil density. Figure 5 summarizes the calculated interfacial thickness values for various systems based on density distribution analyses. Generally, greater interfacial thickness indicated a stronger capacity of surfactants to reduce surface tension.³⁷ In the single 6501 surfactant system, the interfacial film thickness initially increased, followed by a subsequent decrease, with the increment of carbon atoms. For the 126501 system, the interfacial film thickness reached a maximum value of 15.60 Å, while AES demonstrated significant surface tension reduction with an interfacial film thickness of 15.93 Å. In the binary 6501/AES systems, the interfacial thickness improved further, suggesting enhanced interactions between the anionic head groups of AES and water molecules. In the 126501/AES system, the interfacial film thickness increased to 18.08 Å, while both the 146501/AES and 166501/AES systems showed interfacial film thicknesses exceeding 16.00 Å. The dual-component surfactant systems facilitate the formation of a more stable oil repulsion system.

3.2. Diffusion Behavior of Surfactants. The diffusion behavior of surfactants at the oil–water interface can be effectively demonstrated using the mean square displacement (MSD) and the self-diffusion coefficient (D), which are calculated according to eqs 1 and 2, respectively.

$$\text{MSD} = \frac{1}{N_a} \sum_{i=1}^{N_a} \langle [r_i(t) - r_i(0)]^2 \rangle \quad (1)$$

$$D = \frac{1}{6N_a} \lim_{t \rightarrow \infty} \frac{d}{dt} \sum_{i=1}^{N_a} \langle [r_i(t) - r_i(0)]^2 \rangle \quad (2)$$

where N_a is the number of surfactant molecules, and $r_i(t)$ is the position vector of surfactant molecules i at time t .

The movement of surfactant in water within the distance of 6 Å from the polar atoms (S or N) in the surfactant head was analyzed, as 6 Å represents the first hydration layer to the headgroup. Figure 6 illustrates the MSD curves for the surfactants, which show a strong linear relationship over a simulation time of 100 ps, indicating that the system has

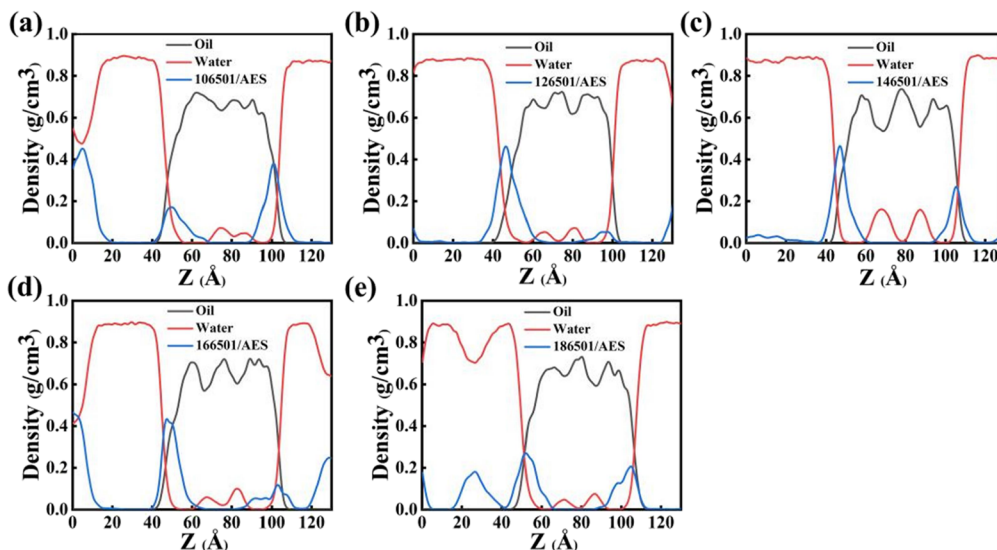


Figure 4. Density distribution of binary surfactants at the oil/water interface: (a) 106501/AES, (b) 126501/AES, (c) 146501/AES, (d) 166501/AES, and (e) 186501/AES.

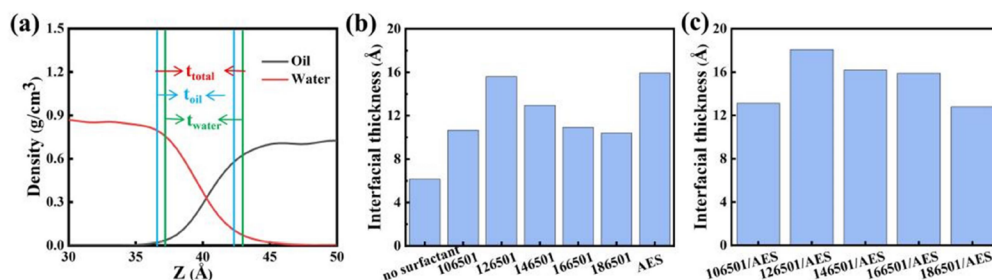


Figure 5. Interfacial thickness of surfactants: (a) schematic diagram, (b) single surfactant, and (c) binary systems.

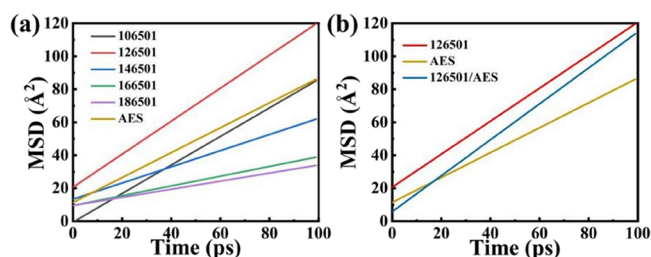


Figure 6. MSD curves of water molecules around surfactant head groups: (a) single surfactant and (b) 126501/AES.

reached equilibrium.³⁹ The slopes of these curves reflect the diffusion capacities of the surfactants. In Figure 6a, 126501 demonstrated the highest diffusion capability. Figure 6b compares the MSD values of individual surfactant systems with their mixtures, revealing that 126501 displayed superior diffusion performance than AES. For the binary surfactant system of 126501/AES, the slope of the MSD increased, indicating improved diffusion properties. The calculated diffusion coefficients for various surfactants are summarized in Table 2. The diffusion coefficient of 126501 was 0.166 Å²/

Table 2. Diffusion Coefficients of Surface Activity in Simulated Systems

surfactant system	diffusion coefficient (Å ² /ps)
106501	0.144
126501	0.166
146501	0.082
166501	0.0493
186501	0.0409
AES	0.125
126501: AES	0.186

ps, which is significantly higher than that of the other 6501 surfactants. For the binary 126501/AES system, the diffusion coefficient increased to 0.186 Å²/ps, surpassing the individual diffusion coefficients of both the 126501 and AES systems.

3.3. Radial Distribution Function of Surfactants in the Oil Layer. The radial distribution function (RDF) characterizes the spatial distribution of oil molecules around a given surfactant molecule. By analyzing $g(r)$, the density of oil molecules around the surfactant molecule was assessed, where an increase in $g(r)$ indicates a stronger interaction between the surfactant and oil molecules. The RDF curves obtained from the simulations are presented in Figure 7. Figure 7a illustrates the RDF values for six individual surfactant systems. All six surfactants exhibited a notable peak around 4.2 Å, which reflected long-range interactions allowing oil molecules to penetrate the surfactant molecules. This finding is consistent

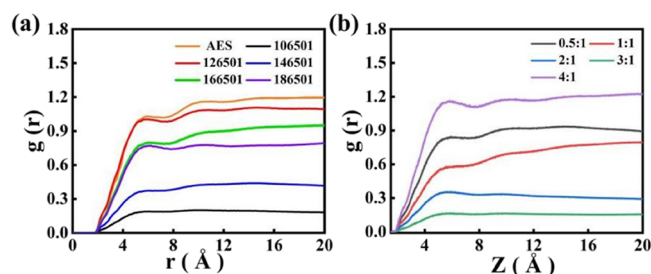


Figure 7. RDF curves of oil molecules around surfactants: (a) single surfactant and (b) 126501/AES with different ratios.

with previous study.⁴⁰ Comparing the $g(r)$ values across these systems revealed the following order of oil molecule presence probability: 106501 < 146501 < 186501 < 166501 < 126501 < AES. Notably, 126501 and AES exhibited the strongest interactions with the oil molecules.

Figure 7b presents the RDF for the binary systems of 126501/AES. When the concentrations of both surfactants were similar, their ability to attract oil molecules was weak. However, when the mixing ratio of 126501 to AES was adjusted to either 4:1 or 0.5:1, the $g(r)$ values increased significantly, indicating the strongest interaction between surfactant molecules and oil molecules. In the high-concentration 126501 nonionic system (4:1 of 126501 to AES), strong hydrogen bonding was present. The addition of AES, with its negatively charged groups, reduced the hydrogen-bonding interactions, thereby facilitating oil molecules' entry into the surfactant layer. Similarly, in the high-concentration AES system (0.5:1 of 126501 to AES), electrostatic repulsion between the AES head groups hindered the entry of oil molecules, and the inclusion of 126501 effectively reduced this electrostatic repulsion, allowing for better penetration of the oil phase.

3.4. Interfacial Characteristics of Binary Surfactants.

Figure 8 shows the interfacial distribution patterns of surfactant mixtures comprising 6501 and AES in a 4:1 ratio after the system reached equilibrium over an extended period (the initial states and NPT optimization results are shown in Figures S1 and S2). The results showed that surfactant molecules can penetrate both the aqueous and oil phases, resulting in a blurred oil–water interface, as previously observed in interfacial science.⁴¹ Furthermore, surfactants that migrated into the oil phase disrupted its ordered structure, which aligned with the literature findings on surfactant-induced structural changes.

Figure 9 illustrates the molecular stretching states of surfactants at the oil–water interface. The surfactants displayed an ordered, tilted distribution at the interface, with the hydrophilic head groups (S and O) oriented toward the water

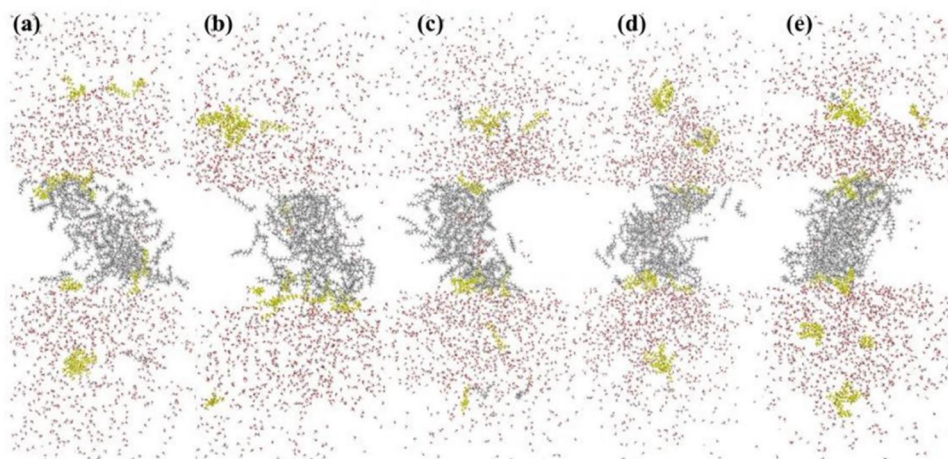


Figure 8. NVT optimization results for a complex surfactant/oil/water system: (a) 106501/AES, (b) 126501/AES, (c) 146501/AES, (d) 166501/AES, and (e) 186501/AES.

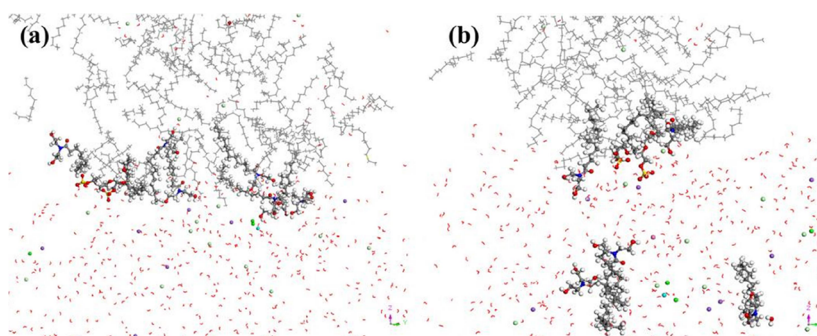


Figure 9. Surfactant adsorption at the oil/water interface: (a) 126501/AES and (b) 186501/AES.

phase and their alkyl chains extending into the oil phase. The ionization of ionic surfactants led to charged molecules at the interface, generating repulsive forces that prevented coalescence as molecules approached each other. Consequently, binary surfactants can effectively and stably distribute at the interface. In Figure 9a, the 126501/AES surfactant system demonstrated a uniform distribution in the interfacial layer, with a substantial number of alkyl chains penetrating the oil phase. This penetration weakened the intermolecular forces within the oil layer, loosening its structure and enhancing its fluidity. In contrast, Figure 9b depicts the 186501/AES system, where surfactants partially remained in the water layer, resulting in a reduced concentration of surfactants at the interface. The limited number of alkyl chains was insufficient to disrupt the intermolecular forces within the oil layer, leading to only slight improvement in its fluidity. These observations underscored the dependence of interfacial dynamics on the surfactant composition and conditions.

3.5. Interfacial Tension and Interfacial Formation Energy of Complex Surfactant Systems. Surface tension is a key indicator for evaluating the effectiveness of enhanced oil recovery. The oil/water interfacial tension of the optimized binary surfactant system was calculated. As shown in Figure 10a, the dual-component system comprising 6501 with a chain length of 12–16 and AES effectively reduced the interfacial tension. Notably, the interfacial tension of the 126501/AES system was reduced to 0.012 mN/m, which was consistent with previous experimental results and met the criteria for effective oil recovery surfactant systems.⁴²

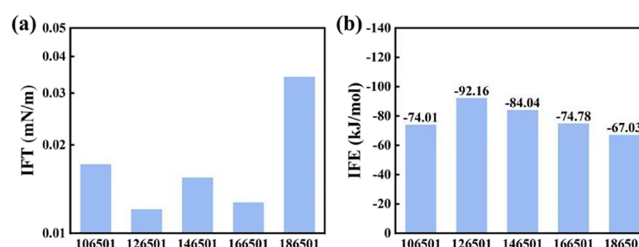


Figure 10. (a) Interfacial tension and (b) interfacial formation energy in the 6501/AES binary systems.

Interfacial energy (IFE) is a direct factor in assessing the stability of interfaces, which can be calculated using the following equation:

$$\text{IFE} = \frac{E_{\text{total}} - (nE_{\text{surfactant}} - E_{\text{decane-water}})}{n} \quad (3)$$

where E_{total} is the total energy of the system when the surfactant system reaches equilibrium at the oil–water interface, $E_{\text{surfactant}}$ is the energy of a single surface-active molecule, $E_{\text{decane-water}}$ indicates the total energy of the system at the oil–water interface when there is no surfactant system, and n is the number of surfactant molecules adsorbed on the oil–water interface.

The introduction of surfactants disrupted the original oil–water interface, resulting in a negative value of IFE. A lower IFE generally indicates a stronger thermodynamic tendency for surfactant adsorption, which is favorable for the formation of a

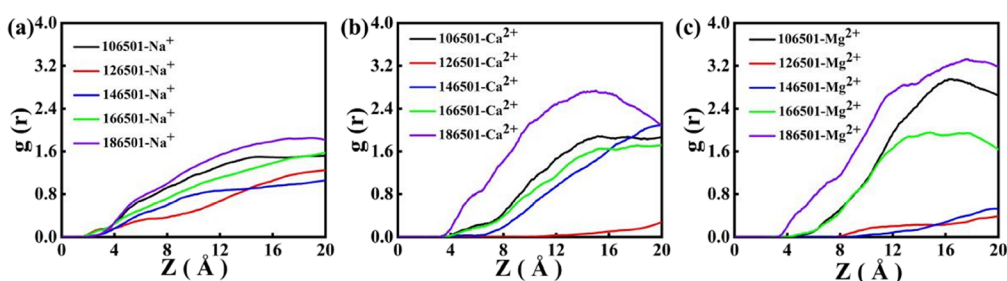


Figure 11. RDF curves of oil molecules around surfactants with cations of (a) Na^+ , (b) Ca^{2+} , and (c) Mg^{2+} .

stable interface. Figure 10b displays the IFE values for various surfactant systems, demonstrating that systems with lower surface tension yield reduced IFE values. Notably, the 126501/AES system exhibited the most stable interface with an IFE of -96.12 kJ/mol, while the 186501/AES system with an IFE of -67.03 kJ/mol showed the least stability. These results highlighted the importance of surfactant molecular characteristics in modulating interfacial stability.

**3.6. Salt Resistance Tests of Surfactant Compound-
ing Systems.** The presence of metal ions in the reservoir can affect the charge distribution and interactions at the oil–water interface, ultimately influencing the oil recovery performance of surfactants.⁴³ Figure 11 depicts the spatial distribution of metal ions near the anionic head groups in various binary surfactant systems. Three cations demonstrated a slight aggregation effect near the anionic head groups, with their distribution initiating at 3 Å and differing significantly by 5 Å. This behavior was attributed to the electrostatic attraction between the negatively charged sulfonate groups of the surfactants and the cations.²⁸ Metal ions were predominantly located in the aqueous phase, particularly at higher concentrations around 10–15 Å. This indicated that the concentration of metal ions remained stable within the interface layer, which showed significant resistance to their presence. A comparison of the three subfigures in Figure 11 revealed that the Na^+ concentration at the interface (3 Å) was higher than that of Ca^{2+} or Mg^{2+} , likely due to the sodium salt structure of the AES surfactant, which increased the local concentration of Na^+ . Peaks for Ca^{2+} and Mg^{2+} were observed around 12 and 15 Å, respectively, while Na^+ gradually reached equilibrium within the aqueous layer. This result reflected the stronger attraction between sulfonate anions and the divalent ions. Furthermore, the carbon chain length of the 6501 surfactant in the binary surfactant systems significantly influenced the distribution of metal ions around the AES anion. The 12-carbon and 14-carbon 6501 systems showed minor variations in the distribution of the three metal ions, whereas the changes in carbon chain length led to an increase in metal ion concentration. Consequently, the 126501/AES and 146,501/AES systems exhibited enhanced resistance to metal ions.

4. CONCLUSIONS

The interfacial properties and molecular adsorption behaviors of 6501 and AES surfactant systems on oil/water surfaces were investigated by using MD simulations. For the nonionic surfactant 6501, it was found that surfactants with either too few or too many carbon atoms negatively affect the interfacial film. Surfactant 126501 with 12 carbon atoms is optimal for chemical flooding. Additionally, the binary surfactant system of 126501/AES improves both the interfacial thickness and the

diffusion coefficient. The ionization of surfactants increases the charge around the interface, generating repulsive forces that stabilize the distribution of the surfactants. The number of alkyl chains in surfactants that penetrate the oil phase contributes to loosening the oil layer. RDF data indicate a significant presence of oil molecules at a 4.2 Å distance from the anionic head of the AES. The low IFE of -96.12 kJ/mol in 126501/AES promotes a stable interface. Moreover, both the 126501/AES and 146501/AES systems exhibit excellent resistance to metal ions. These findings highlight the importance of selecting the appropriate carbon chain length for nonionic surfactants as oil recovery, with binary surfactants enhancing oil recovery performance.

■ ASSOCIATED CONTENT

Supporting Information

The Supporting Information is available free of charge at <https://pubs.acs.org/doi/10.1021/acsomega.4c11148>.

Calculated parameters for molecular dynamics simulations (Table S1); modeling the quantities of components in a complex system (Table S2); initial state of the water/surface/oil (a) 106501/AES, (b) 126501/AES, (c) 146501/AES, (d) 166501/AES, and (e) 186501/AES (Figure S1); and NPT optimization results of water/surface/oil (a) 106501/AES, (b) 126501/AES, (c) 146501/AES, (d) 166501/AES, and (e) 186501/AES (Figure S2) (PDF)

■ AUTHOR INFORMATION

Corresponding Authors

Zhaojun Chen — State Key Laboratory of Shale Oil and Gas Enrichment Mechanisms and Effective Development, Beijing 102206, China; Research and Development Center for the Sustainable Development of Continental Sandstone Mature Oilfield by National Energy Administration, Beijing 100824, China; College of Chemistry and Chemical Engineering, Institute for Sustainable Energy and Resources, Qingdao University, Qingdao, Shandong 266000, China; orcid.org/0009-0002-1180-3119; Email: chenzj_upc@126.com

Jinpan Zhong — State Key Laboratory of Shale Oil and Gas Enrichment Mechanisms and Effective Development, Beijing 102206, China; Research and Development Center for the Sustainable Development of Continental Sandstone Mature Oilfield by National Energy Administration, Beijing 100824, China; Petroleum Exploration and Production Research Institute, SINOPEC, Beijing 100083, China; Email: zhongjp.syky@sinopec.com

Authors

Yangwen Zhu – State Key Laboratory of Shale Oil and Gas Enrichment Mechanisms and Effective Development, Beijing 102206, China; Research and Development Center for the Sustainable Development of Continental Sandstone Mature Oilfield by National Energy Administration, Beijing 100824, China; Petroleum Exploration and Production Research Institute, SINOPEC, Beijing 100083, China

Ping Liu – State Key Laboratory of Shale Oil and Gas Enrichment Mechanisms and Effective Development, Beijing 102206, China; Research and Development Center for the Sustainable Development of Continental Sandstone Mature Oilfield by National Energy Administration, Beijing 100824, China; Petroleum Exploration and Production Research Institute, SINOPEC, Beijing 100083, China

Yong Wang – State Key Laboratory of Shale Oil and Gas Enrichment Mechanisms and Effective Development, Beijing 102206, China; Research and Development Center for the Sustainable Development of Continental Sandstone Mature Oilfield by National Energy Administration, Beijing 100824, China; Petroleum Exploration and Production Research Institute, SINOPEC, Beijing 100083, China

Hongmin Yu – State Key Laboratory of Shale Oil and Gas Enrichment Mechanisms and Effective Development, Beijing 102206, China; Research and Development Center for the Sustainable Development of Continental Sandstone Mature Oilfield by National Energy Administration, Beijing 100824, China; Petroleum Exploration and Production Research Institute, SINOPEC, Beijing 100083, China

Li Zhang – State Key Laboratory of Shale Oil and Gas Enrichment Mechanisms and Effective Development, Beijing 102206, China; Research and Development Center for the Sustainable Development of Continental Sandstone Mature Oilfield by National Energy Administration, Beijing 100824, China; Petroleum Exploration and Production Research Institute, SINOPEC, Beijing 100083, China

Luxuan Ma – College of Chemistry and Chemical Engineering, Institute for Sustainable Energy and Resources, Qingdao University, Qingdao, Shandong 266000, China

Deshuai Sun – College of Chemistry and Chemical Engineering, Institute for Sustainable Energy and Resources, Qingdao University, Qingdao, Shandong 266000, China; orcid.org/0000-0002-4187-8886

Kai Xia – College of Chemistry and Chemical Engineering, Institute for Sustainable Energy and Resources, Qingdao University, Qingdao, Shandong 266000, China

Complete contact information is available at:
<https://pubs.acs.org/10.1021/acsomega.4c11148>

Notes

The authors declare no competing financial interest.

ACKNOWLEDGMENTS

This work was supported by the Open Foundation of Research and Development Center for the Sustainable Development of Continental Sandstone Mature Oilfield by National Energy Administration (KLP23025).

REFERENCES

- (1) Delannoy, L.; Longaretti, P.-Y.; Murphy, D. J.; Prados, E. Peak oil and the low-carbon energy transition: A net-energy perspective. *Applied Energy* **2021**, 304, No. 117843.
- (2) Zhang, L.; Luo, L.; Zhao, S.; Yu, J. Studies of Synergism/Antagonism for Lowering Dynamic Interfacial Tensions in Surfactant/Alkali/Acidic Oil Systems, Part 2: Synergism/Antagonism in Binary Surfactant Mixtures. *J. Colloid Interface Sci.* **2002**, 251 (1), 166–171.
- (3) Gbadamosi, A. O.; Kiwalabye, J.; Junin, R.; Augustine, A. A review of gas enhanced oil recovery schemes used in the North Sea. *Journal of Petroleum Exploration and Production Technology* **2018**, 8 (4), 1373–1387.
- (4) Massarweh, O.; Abushaikh, A. S. The use of surfactants in enhanced oil recovery: A review of recent advances. *Energy Reports* **2020**, 6, 3150–3178.
- (5) Chen, L.; Xiao, J. X.; Ma, J. M. Striking differences between alkyl sulfate and alkyl sulfonate when mixed with cationic surfactants. *Colloid Polym. Sci.* **2004**, 282 (5), 524–529.
- (6) Yan, P.; Xiao, J. X. Polymer-surfactant interaction: differences between alkyl sulfate and alkyl sulfonate. *Colloids Surf., A* **2004**, 244 (1–3), 39–44.
- (7) Shi, P.; Zhang, H.; Lin, L.; Song, C.; Chen, Q.; Li, Z. Molecular dynamics simulation of four typical surfactants at oil/water interface. *J. Dispersion Sci. Technol.* **2018**, 39 (9), 1258–1265.
- (8) Kunieda, M.; Nakaoka, K.; Liang, Y. F.; Miranda, C. R.; Ueda, A.; Takahashi, S.; Okabe, H.; Matsuoka, T. Self-accumulation of aromatics at the oil-water interface through weak hydrogen bonding. *Journal of The American Chemical Society* **2010**, 132 (S1), 18281–18286.
- (9) Ding, L.; Wu, Q. H.; Zhang, L.; Guérillot, D. Application of fractional flow theory for analytical modeling of surfactant flooding, polymer flooding, and surfactant/polymer flooding for chemical enhanced oil recovery. *Water* **2020**, 12 (8), 2195.
- (10) Xu, Y. F.; Wang, Z. H.; Han, X.; Hong, J. J.; Wang, Y. Impact of sodium dodecyl benzene sulfonate concentration on the stability of the crude oil-mineral water interfacial film: a molecular dynamics simulation study. *Energy Fuels* **2022**, 36 (8), 4358–4369.
- (11) Pal, N.; Saxena, N.; Mandal, A. Studies on the physicochemical properties of synthesized tailor-made gemini surfactants for application in enhanced oil recovery. *J. Mol. Liq.* **2018**, 258, 211–224.
- (12) Pal, N.; Saxena, N.; Divya Laxmi, K. V.; Mandal, A. Interfacial behaviour, wettability alteration and emulsification characteristics of a novel surfactant: Implications for enhanced oil recovery. *Chem. Eng. Sci.* **2018**, 187, 200–212.
- (13) Kesarwani, H.; Saxena, A.; Mandal, A.; Sharma, S. Anionic/nonionic surfactant mixture for enhanced oil recovery through the investigation of adsorption, interfacial, rheological, and rock wetting characteristics. *Energy Fuels* **2021**, 35 (4), 3065–3078.
- (14) Sheng, S.-S.; Cao, X.-L.; Zhu, Y.-W.; Jin, Z.-Q.; Zhang, L.; Zhu, Y.; Zhang, L. Structure-activity relationship of anionic-nonionic surfactant for reducing interfacial tension of crude oil. *J. Mol. Liq.* **2020**, 313, No. 112772.
- (15) Wang, Y.; Hou, B.; Cao, X.; Zhang, J.; Song, X.; Ding, M.; Chen, W. Interaction between polymer and anionic/nonionic surfactants and its mechanism of enhanced oil recovery. *J. Dispersion Sci. Technol.* **2018**, 39 (8), 1178–1184.
- (16) Lu, S. H.; Somasundaran, P. Tunable synergism/antagonism in a mixed nonionic/anionic surfactant layer at the solid/liquid interface. *Langmuir* **2008**, 24 (8), 3874–3879.
- (17) Shang, B. Z.; Wang, Z. W.; Larson, R. G. Molecular dynamics simulation of interactions between a sodium dodecyl sulfate micelle and a poly (ethylene oxide) polymer. *J. Phys. Chem. B* **2008**, 112 (10), 2888–2900.
- (18) Yuan, S.; Wang, S.; Wang, X.; Guo, M.; Wang, Y.; Wang, D. Molecular dynamics simulation of oil detachment from calcite surface in aqueous surfactant solution. *Computational and Theoretical Chemistry* **2016**, 1092, 82–89.
- (19) Ivanova, A. A.; Koltsov, I. N.; Groman, A. A.; Cheremisin, A. N. Molecular dynamics simulations for surfactant research. *Petroleum Chemistry* **2023**, 63 (8), 867–885.
- (20) Lu, C.; Xu, X.; Yuan, Z.; Liu, J.; Li, S.; Liu, W.; Wang, H.; Gao, Q.; Ding, W. Molecular dynamic simulation study on effect of

anionic–nonionic surfactants on decane desorption from SiO₂ surface. *J. Mol. Liq.* **2024**, *414*, No. 126162.

(21) LÜ, D.; Wu, H.; Chen, J.; Nie, Y.; Bian, G.; Li, J.; Gong, S. Research progress of molecular dynamics simulation on adsorption mechanisms of dispersants/surfactants on the surface of coal particles. *J. Fuel Chem. Technol.* **2024**, *52* (3), 452–460.

(22) Wu, X.; Xia, Y.; Yuan, L.; Yuan, R.; He, X. Molecular dynamics simulations of the molecular behavior and synergistic effect of anionic/zwitterionic surfactants at oil–water interface. *Acta Petrol. Sin.* **2021**, *37* (4), 831–839.

(23) Xu, J.; Zhang, Y.; Chen, H.; Wang, P.; Xie, Z.; Yao, Y.; Yan, Y.; Zhang, J. Effect of surfactant headgroups on the oil/water interface: An interfacial tension measurement and simulation study. *J. Mol. Struct.* **2013**, *1052*, 50–56.

(24) Jang, S. S.; Lin, S.-T.; Maiti, P. K.; Blanco, M.; Goddard, W. A.; Shuler, P.; Tang, Y. Molecular dynamics study of a surfactant-mediated decane–water interface: effect of molecular architecture of alkyl benzene sulfonate. *J. Phys. Chem. B* **2004**, *108* (32), 12130–12140.

(25) Lian, P.; Jia, H.; Yan, H.; Yuan, J.; Tang, H.; Li, Z.; Fan, F.; Qin, X.; Lv, K.; Liu, D. Effects of micellization behavior on the interfacial adsorption in binary anionic/nonionic surfactant systems: a molecular simulation study. *Langmuir* **2021**, *37* (40), 11835–11843.

(26) Xian, X. K.; Ye, Z. B.; Tang, L.; Wang, J. Q.; Lai, N. J.; Xiao, B.; Wang, Z. X.; Li, S. L. Molecular dynamics simulation of the effects of complex surfactants on oil–water interaction and aggregation characteristics at the interface. *Langmuir* **2023**, *39* (39), 14130–14138.

(27) Zhou, W.; Jiang, L.; Liu, X.; Hu, Y.; Yan, Y. Molecular insights into the effect of anionic–nonionic and cationic surfactant mixtures on interfacial properties of oil–water interface. *Colloids Surf., A* **2022**, *637*, No. 128259.

(28) Cai, H. Y.; Zhang, Y.; Liu, Z. Y.; Li, J. G.; Gong, Q. T.; Liao, Q.; Zhang, L.; Zhao, S. Molecular dynamics simulation of binary betaine and anionic surfactant mixtures at decane–water interface. *J. Mol. Liq.* **2018**, *266*, 82–89.

(29) Pal, N.; Saxena, N.; Mandal, A. Equilibrium and dynamic adsorption of gemini surfactants with different spacer lengths at oil/aqueous interfaces. *Colloids Surf., A* **2017**, *533*, 20–32.

(30) Biovia, D. S. *Discovery Studio Modeling Environment*; Dassault Systèmes, 2020.

(31) Ahmad, Z. U.; Chao, B.; Konggidinata, M. I.; Lian, Q. Y.; Zappi, M. E.; Gang, D. D. Molecular simulation and experimental validation of resorcinol adsorption on ordered mesoporous carbon (OMC). *Journal of Hazardous Materials* **2018**, *354*, 258–265.

(32) Sun, H.; Ren, P.; Fried, J. R. The COMPASS force field: parameterization and validation for phosphazenes. *Comput. Theor. Polym. Sci.* **1998**, *8* (1), 229–246.

(33) Liu, Z.; Li, X.; He, W.; Zhao, G.; Yang, Y.; Liu, X.; Zhang, X.; Li, X.; Zhang, S.; Sun, W.; Lu, G. Synergistic effect of charge and strain engineering on porous g-C₃N₇ nanosheets for highly controllable CO₂ capture and separation. *Sep. Purif. Technol.* **2022**, *282*, No. 120135.

(34) Baidakov, V. G.; Chernykh, G. G.; Protsenko, S. P. Effect of the cut-off radius of the intermolecular potential on phase equilibrium and surface tension in Lennard–Jones systems. *Chem. Phys. Lett.* **2000**, *321* (3), 315–320.

(35) Hou, J. J.; Lin, S. L.; Du, J. Z.; Sui, H. Study of the adsorption behavior of surfactants on carbonate surface by experiment and molecular dynamics simulation. *Front. Chem.* **2022**, *10*, No. 847986.

(36) Tan, J. S. J.; Zhang, L.; Lim, F. C. H.; Cheong, D. W. Interfacial properties and monolayer collapse of alkyl benzenesulfonate surfactant monolayers at the decane–water interface from molecular dynamics simulations. *Langmuir* **2017**, *33* (18), 4461–4476.

(37) Luo, G.; Malkova, S.; Pingali, S. V.; Schultz, D. G.; Lin, B.; Meron, M.; Graber, T. J.; Gebhardt, J.; Vanysek, P.; Schlossman, M. L. The width of the water/2-heptanone liquid–liquid interface. *Electrochem. Commun.* **2005**, *7* (6), 627–630.

(38) Cao, Y.; Zhao, R.-h.; Zhang, L.; Xu, Z.-c.; Jin, Z.-c.; Luo, L.; Zhang, L.; Zhao, S. Effect of electrolyte and temperature on interfacial tensions of alkylbenzene sulfonate solutions. *Energy Fuels* **2012**, *26*, 2175–2181.

(39) Mahfud, R. Molecular dynamics computational study of sustainable green surfactant for application in chemical enhanced oil recovery. *ACS Omega* **2024**, *9* (25), 27177–27191.

(40) Wang, Y. Oil displacement performance of alkanolamide surfactants and its compound system for high calcium and magnesium reservoirs. *Petrol. Drill. Tech.* **2018**, *46* (3), 98–102.

(41) Yang, Y.; Ma, Z.; Xia, F.; Li, X. Adsorption behavior of oil-displacing surfactant at oil/water interface: Molecular simulation and experimental. *Journal of Water Process Engineering* **2020**, *36*, No. 101292.

(42) Numin, M. S.; Hassan, A.; Jumbri, K.; Ramli, A.; Borhan, N. Interfacial tension reduction mechanism by alkaline-surfactant-polymer at oil–water interface from experimental and molecular dynamics approaches. *J. Mol. Liq.* **2022**, *356*, No. 119006.

(43) Lin, Y.; Tang, W.; Xiao, P.; Ma, J.; Han, X.; Xu, X.; Luo, J.; Zhao, S. Synergistic effect of salt and anionic surfactants on interfacial tension reduction: insights from molecular dynamics simulations. *Langmuir* **2023**, *39* (35), 12392–12401.